Available online at www.jrors.ir

Journal Of Radar and Optical Remote Sensing

JRORS 2 (2020) 7–22

Comparison of MODIS, SEVIRI and INSAT-3D Land Surface Temperature (LST)

Mehdi Gholamnia[a*], Salman Ahmadi[b], Reza Khandan[c], Seyed Kazem Alavipanah[d], Ali Darvishi Boloorani[e], Saeid Hamzeh[e]

[a]*Department of Civil Engineering, Sanandaj Branch, Islamic Azad University,Sanandaj, Iran*

[b]*Assistant Professor of Eengineering Faculty, University of Kurdistan*

[c]*Faculty of Geography, Department of Remote Sensing and GIS, University of Tehran, Iran*

[d]*Professor, Faculty of Geography, Department of Remote Sensing and GIS, University of Tehran, Iran*

[e]*Assistant Professor, Faculty of Geography, Department of Remote Sensing and GIS, University of Tehran, Iran*

Received 17 March 2020; revised 5 May 2020; accepted 22 June 2020

Abstract

The accuracy of retrieved LST from satellites is of great importance. Among different LST validation methods, a cross-calibration procedure is highly cost-effective and applicable. The Indian National Satellite-3D series (INSAT-3D) and Meteosat Second Generation (MSG) are two geostationary satellites that which provide LST products with high temporal resolution. Considering MODIS as the reference (polar orbit that is onboard Aqua and Terra satellites), the comparison of the LST products of these geostationary satellites was evaluated from 4th March to 1st September 2015. For this purpose mean LST ratios were calculated for both MODIS-Imager (from INSAT-D) and MODIS-SEVIRI. Then the behavior of their mean LST ratio was analyzed for the exciting four major land covers and five elevation classes in the study area. The results showed that Imager data underestimated and overestimated the LST in comparison to MODIS data during the day and night time respectively. The SEVIRI LSTs underestimated the LST in both day and night time in comparison with MODIS products. In order to model the discrepancies between MODIS-Imager and MODIS-SEVIRI, for each land cover a multilinear regression model was fitted based on slope, aspect, azimuth, and View Zenith Angle (VZA). The results showed that barren, Shrub, grass, and cereal crops had low RMSEs in model fitting, respectively.

Keywords*:* LST, Geostationary Satellite, Land cover, Elevation, Remote Sensing

1. Introduction

Land Surface Temperature (LST) is a key variable for many studies including land surface modeling (Jin, 2004; Norman and Becker, 1995; Alavipanah et al, 2010), monitoring of land surface conditions

* Corresponding author Tel: +98- 9181735227.
Email address: mehgholamnia@gmail.com

(Xu et al, 2011; Wang et al, 2014), evapotranspiration, climate change, hydrological cycle, vegetation monitoring and urban studies (Weng, 2009; Li et al, 2013). The LST can be retrieved from both polar and geostationary platforms with different spatial and temporal characteristics. The accuracy of retrieved LST from satellite imagery is influenced by plenty of variables such as spectral functions of thermal bands, channel emissivity, atmospheric attenuation modeling, sensor noise, angular anisotropy, weights of components within a pixel, temperature range, view zenith angle (VZA) and topographic issues like slop and aspect (Li et al, 2013). Generally, there are four methods for LST validation as following; 1. Temperature-based, 2. Radiance-based, 3. Indirect validation, and 4. Cross-validation (Tang and Li, 2013). The first three methods have some limitations and are dependent on ground measurements. Satellite-based cross-calibration is the comparison of LST values retrieved by methods under test with well-documented and validated LSTs by other satellites (Trigo et al, 2008). Satellite based cross calibration is an effective method for LST validation in large and out-of-reach. Trigo et al. (2008) addressed the discrepancies between MODIS and Spinning Enhanced Visible and infrared imager (SEVIRI) onboard MSG and analyzed the sources of such ratio in three aspects: 1) satellite viewing angle differences, 2) surface topography, and 3) surface type. Higher differences in LST observations were found for heterogeneous surfaces either in terms of topography or land cover. Gao et al. (2012) compares the LSTs of SEVIRI and MODIS. Higher discrepancies are shown in the daytime especially for arid regions. The nature of such a ratio can be attributed to time, land cover, and VZA. In EPSA (2014) MODIS and Imager (INSAT-3D) LSTs were compared on 29th November 2013. The results show R2 values of 0.73 (05:30 GMT), 0.66 (09.00 GMT) and 0.79 (21:00 GMT). Such comparisons were on a specific area and land covers. It is preferable to evaluate these products over Iran which has different land covers and elevations. The study of the discrepancies between geostationary satellites and MODIS can be of great help in many research topics in Iran.

This study attempted to justify and model the discrepancies by cross-calibration between MODIS and two geostationary satellites INSAT-3D and MSG LSTs in different land covers and elevations.

2. Material and Methods

2.1. Study Area

The area of this study was the joint covered area by both Imager and SEVIRI satellite date over Iran. It is extended from the 43° to 64° East and 25° to 40° North (Figure 1). According to the De Martonn climate classification method, Iran has 65% dry, 20% semiarid, and 10% humid climate regions (Katiraie-Boroujerdy et al, 2013). Iran is affected by Siberian high pressure from North, Mediterranean low pressure from the west, and Sudan low pressure from the south(Golestanil et al, 2000).

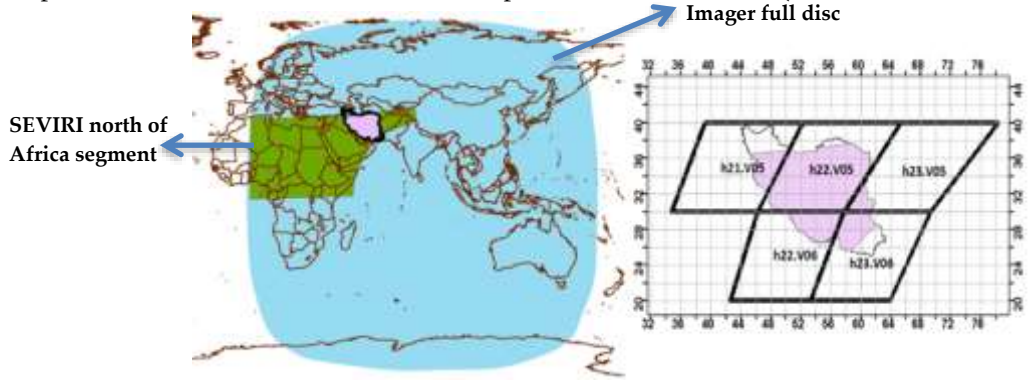

Figure 1. A) study area covered by Imager and SEVIRI; B) frames of MODIS data over the study area

2.2. Data Set

MODIS Data

MODIS data of Aqua and Terra satellites are available since 5th March 2000 and 8th July 2002 respectively. MODIS L3 LST products (MOD11A1 and MYD11A2) are produced in 5 frames h21.V05, h22.V05, h23.V05, h22.V06, and h23.V06 over study area (Figure 1B). LST products have 1 km spatial resolution and are available four times a day for study area by Aqua (daily products known as MYD-D and nightly products known as MYD-N) and Terra (daily products known as MOD-D and nightly products known MOD-N)(Wan, 2008). The time series of LST were downloaded for the study area based on mentioned frames from 4th March 2015 to 1st September 2015.

MODIS 500m land cover products MCD12Q1 derived from yearly observations of both Aqua and Terra. It contains five land cover classification schemes extracted through a supervised decision-tree classification method: 1) IGBP global vegetation classification scheme, 2) University of Maryland (UMD) scheme, 3) MODIS-derived LAI/FPAR scheme, 4) MODIS-derived Net Primary Production (NPP) scheme; 5) Plant Functional Type (PFT) scheme. Considering the study area, the fifth land cover type was chosen for this study (Figure 2).

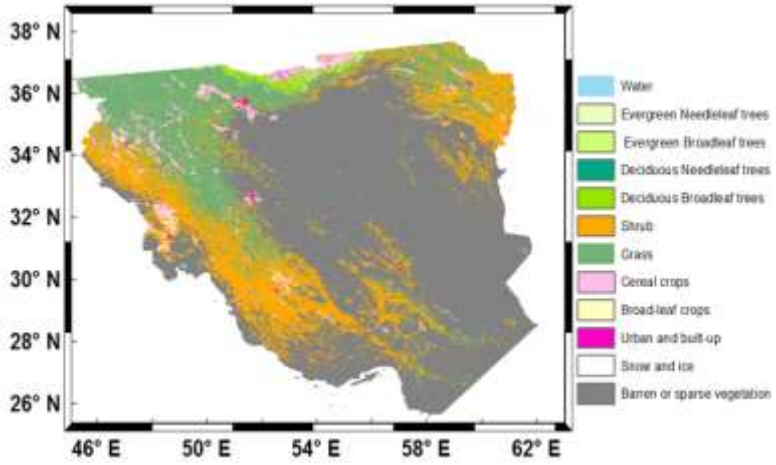

Figure 2. Fifth land cover type of MCD12Q1 over Iran

Imager Data

Imager onboard INSAT3-D geostationary satellite is located on 84º East on the equator. Half hourly LST data from this sensor is available since 4th March 2015 through http://mosdac.gov.in. In this study, 7044 LST products from 4th March to 1st September 2015 were downloaded. LST products are in H5 format and the view angle of this satellite varies between 39.11 and 55.57 (Figure 3A). Coefficients of the Imager LST retrieval algorithm were calculated based on MODerate resolution atmospheric TRANsmission (MODRAN) radiative transfer model simulations by considering five variables: 1. Atmospheric lower boundary temperature simulations over the tropical region, 2. Atmospheric column water vapor, 3. Surface temperature (260-330 K), 4. VZA 0-60 degrees and 5.

SEVIRI Data

SEVIRI onboard (MSG) is located 0 degrees east over the equator. LST products of this sensor are available from 1st January 2009 via http://landsaf.ipma.pt. In this paper, 21127 LST products with 15-

minute temporal resolutions were used from 4th March to 1st September 2015. Satellite VZA changes between 61.82 to 75.41 degrees over the study area (Figure 3B). Sobrino and Romaguera (2004) estimated LST errors for different view angles through simulated radiances by MODTRAN3. Based on the results of simulations, they proposed different coefficients for view angles 0, 10, 20, 30, 40, 50, and 60 degrees. Therefore, in Generalized Split Window (GSW) algorithm the effects of VZA have been considered.

Table 1. Comparison of thermal bands in three sensors MODIS, SEVIRI, and Imager (Aminou 2002; Pandya et al. 2011; Wan 2006)

Sensor	Orbit	Band number for TIR1	Band number for TIR2	Wavelength range of TIR1	Spectral range of TIR2	Radiometric resolution	Spatial resolution (near nadir)	Temporal resolution
MODIS	Polar	31	32	10.78-11.28	11.77-12.02	16 bit	1 (km)	4 times a day
Imager	Geostationary	5	6	10.30-11.30	11.50-12.50	10 bit	4(km)	Half hour
SEVIRI	Geostationary	9	10	9.80-11.80	11.00-13.00	10 bit	3.3(km)	Half hour

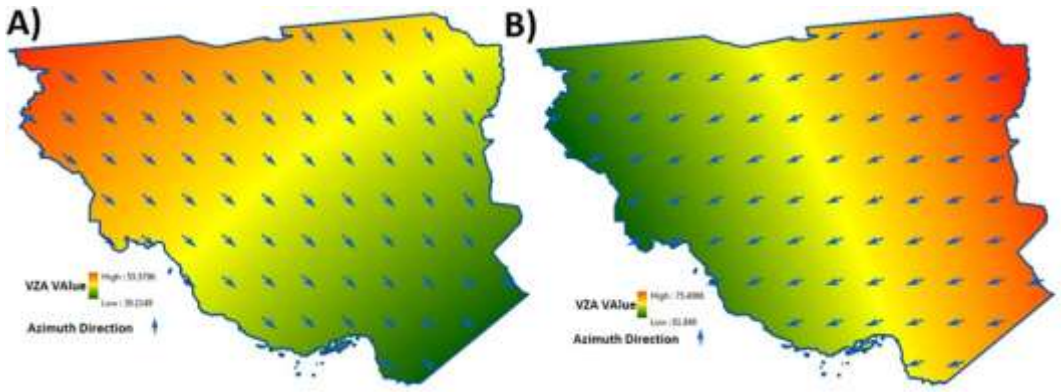

Figure 3. VZA and azimuth direction of A) Imager and B) SEVIRI (the arrows show the direction from pixels toward sensor)

Elevation Data

Elevation data from ASTER with 30 m resolution for the study area were downloaded via. The elevation data in study area were classified in five classes (Figure 4).

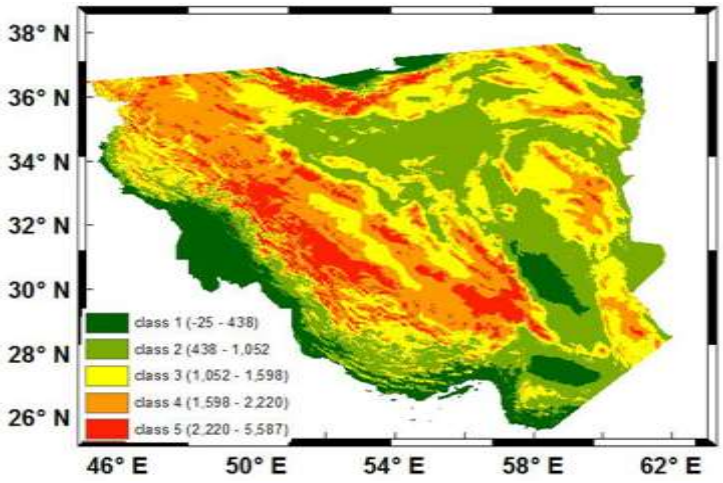

Figure 4. Topography classification in the study area

3. Methodology

The LST time series of SEVIRI and Imager sensors from 4th March 2015 till 1st September 2015 were extracted. The reason for the selection of this period is that Imager LSTs were available since 4th March 2015. Extracted information includes skin temperature, time, sensor VZA, and data quality. LST retrieval methods of MODIS and SEVIRI sensors are based on Wan and Dozier (1996) (RMI Team 2011; Wan 2016). LST retrieval of Imager is based on the following equation(EPSA 2014).

$$\mathrm{LST} = \alpha_1 \mathrm{TIR}_1 + \alpha_2(\mathrm{TIR}_1 - \mathrm{TIR}_2) + \alpha_3(\mathrm{TIR}_1 - \mathrm{TIR}_2)^2 + \alpha_4(1-\varepsilon) + \alpha_5\,\Delta\varepsilon + \alpha_6 \qquad (2)$$

Where TIR1 and TIR2 are brightness temperatures of Imager thermal bands, ε is emissivity which is based on MODIS emissivity products, Δε is the difference of emissivity for two thermal bands. α_1 to α_6 are coefficients. In order to reduce the effect of angular anisotropy, these coefficients were calculated for different VZAs (more details in (EPSA 2014)). In the next step, the times of MODIS LST products were converted to GMT and concurrent LST products with SEVIRI and Imager were selected. Because MODIS sensor in this study chosen as a reference, only pixels of MODIS which had VZAs less than 40 degrees (near nadir pixels) were extracted. Based on the VZAs, the distance between pixel centers of Imager varies between 6.5 to 7 Km, and for SEVIRI changes between 4.8 and 5.7 km in the study area. Therefore, all the LSTs products of these three sensors were resampled to 7 km. By resampling Imager and SEVIRI LSTs, co-located pixels showed more than 80% coverage. In order to decrease the high cost of computation required for cross-comparison of pixels in the field of view of sensors, a total number of 16428 which were normally distributed were selected. Based on the spatial resolution of SEVIRI and Imager, MODIS LSTs were resampled to 7km. Then, LSTs of MODIS were divided by Imager and SEVIRI for corresponding pixels for the whole time series. Finally, by removing the outlier data with a 95% confidence interval (using the ratio histograms of each pixel during the time series), the mean LST ratio was calculated by the mean of pixel values during the time series for each pixel. In order to evaluate the results of LST means ratios, time series were divided into two equal periods and LST means ratios of each period were compared. Then, mean LST ratios were analyzed concerning the land cover maps and elevation data. The Land cover map contains 12 classes and minor classes like water, snow, and ice, evergreen needle leaf trees, evergreen broadleaf trees, deciduous needle leaf trees, deciduous broadleaf trees, urban and built-up, Broad-leaf crops were excluded from calculations. The used classes (Shrubs, Grass, Cereal crops, and Barren or sparse vegetation) cover 97.78% of the

study area. The mean LST ratios were interpreted based on the variability of land covers and elevation classes. A multilinear regression model was fitted to Mean LST ratios, as a dependent variable, and VZA, azimuth angle, slope, aspect, and elevation, as independent variables using half of the data set (8214 pixels). The Azimuth angle is defined as the horizontal angle between the north and pixel-satellite direction for each pixel. For each satellite pair observation and land cover, a multilinear regression model was calculated; 32 regression models were fitted. Finally, the second half part of the dataset was used as a test for validation of regression models (Figure 5).

4. Results

Figures 6 and 7 show the map results of the LST mean ratios extracted for the whole time series of each satellite pair. The results from these maps show some spatial differences which were analyzed by land cover and elevation classes in the 4.1 and 4.2 sections. As mentioned earlier, the whole time series of LSTs were divided for two purposes: 1) to test how much the ratios are reliable and 2) to validate the multilinear regression relations. Regarding the first purpose, Figure (8) shows the histograms of mean ratio differences for two-time periods (the differences between ratios of two time series). The results showed that histograms (for both satellite pairs) were normal and had low errors; the mean differences of LST mean ratios were near zero. The Standard Deviations (STD) in MODIS-Imager daily observations were higher than nightly observations. The STDs in MODIS-SEVIRI daily observations were lower than nightly ones.

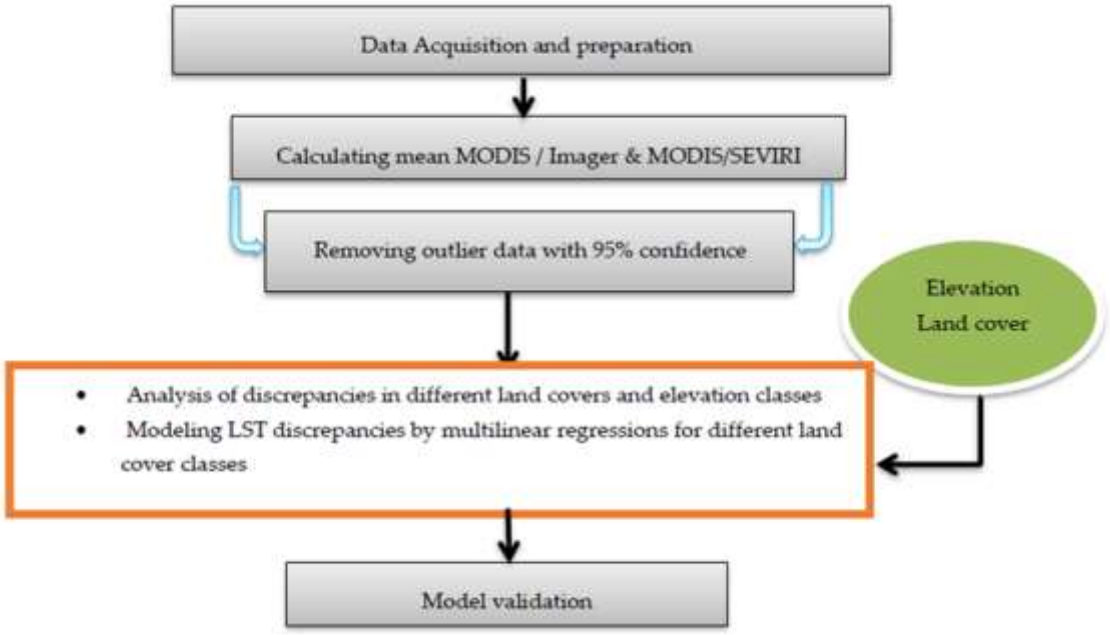

Figure 5. Flowchart of analyzing and modeling LST ratios

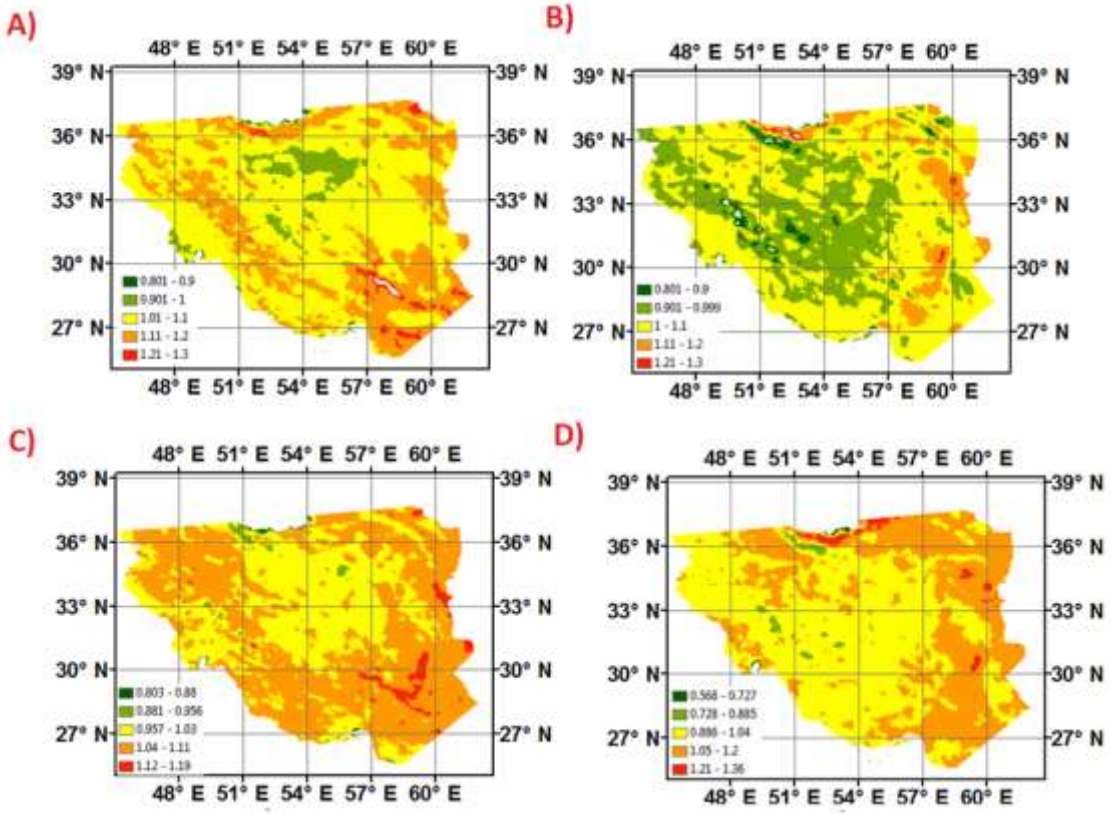

Figure 6. Mean LST ratios for MODIS-SEVIRI; A) daily MODIS (onboard Terra) divided by SEVIRI; B) nightly MODIS (onboard Terra) divided by SEVIRI; C) daily MODIS (onboard Aqua) divided by SEVIRI; D) nightly MODIS (onboard Aqua) divided by SEVIRI

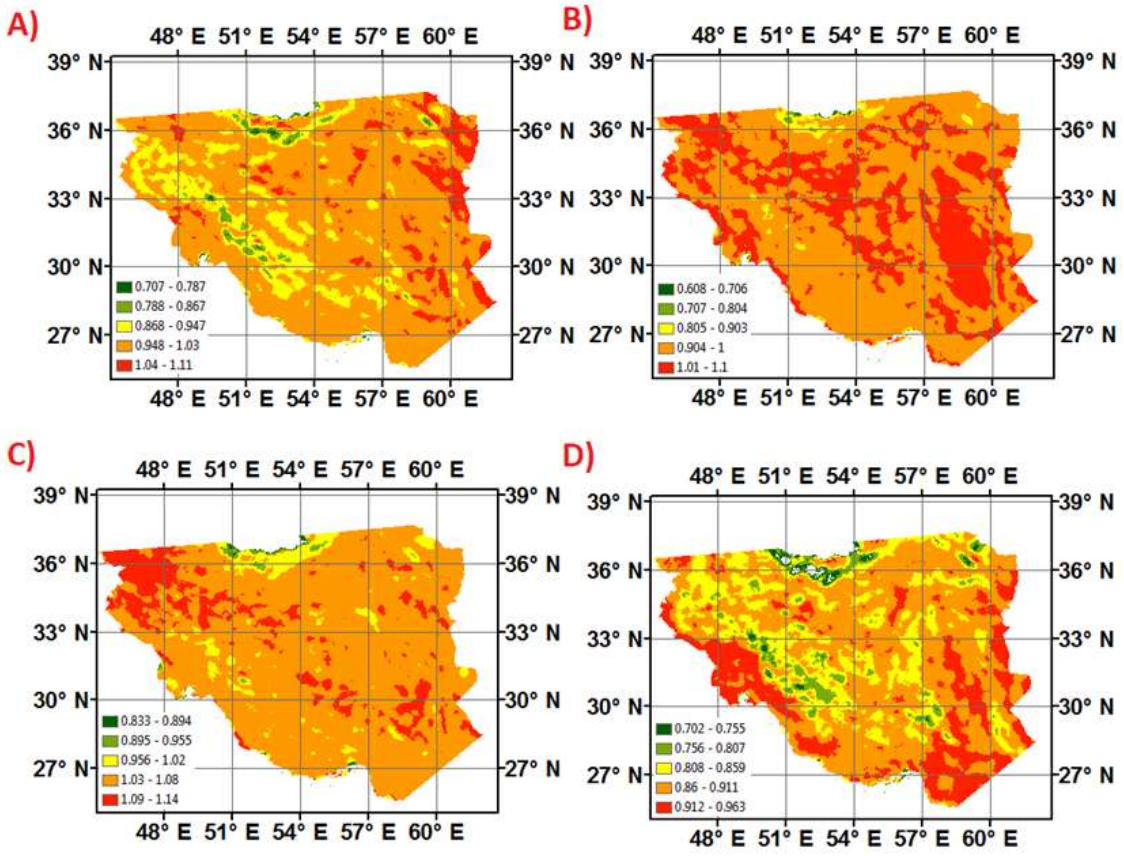

Figure 7. Mean LST ratios for MODIS-Imager; A) daily MODIS divided by IMAGER; B) nightly MODIS divided by IMAGER; C) daily MODIS divided by IMAGER; D) nightly MODIS divided by IMAGER

In order to analyze the effect of land cover on mean LST ratios (Figure 6 and 7), MODIS-Imager and MODIS-SEVIRI LST mean ratios and STDs were plotted in four elevation classes.

4.1. Analysis of MODIS-Imager

The LST mean ratio analysis of MOD-D, MYD-N, MYD-D, and MOD-N for different land covers and elevation classes are summarized in Figures 9 and 10. In Figure 9, results show that, during daytime, the ratios are higher, especially near amplitude LST time which was observed by MYD-D (around 13:30 local time). On the other hand, the more the LST increases, the more the mean LST ratios increase for all four land types. During night time MYD-N (01:30 local time) showed ratios less than 1 indicating that MODIS LSTs during night time were lower than Imager ones. MOD-D (around 10:00 local time) and MOD-N (around 22:00 local time) are almost close to each other. Another point that is clear in all plots especially in barren land cover is the decrease of LST mean ratio by an elevation increase. In fact, as elevation increases the Imager showed larger LST values in contrast with MODIS. The standard deviation analysis of mean LST ratios in Figure (10) showed that elevation increase caused those Mean LST ratios to get distance from the mean. It indicated that topography was an important factor in the variability of LST values. Such variability had almost the same rate for land covers shrub, barren, and grass.

4.2. Analysis of MODIS-SEVIRI

The results of the MODIS-SEVIRI analysis are given in Figure 11. As this figure shows during both day and night MODIS LST values were larger than SEVIRI LSTs in low elevation lands (less than class 3). In the fourth and fifth classes of elevation, the mean LST ratios MOD-D were the largest. MOD-D and MYD-D did not show a specific behavior with elevation but MOD-N and MYD-N had a relation with elevation and in higher terrains, the MODIS LST values tended to be lower than SEVIRI values. Figure (12) shows STD in shrub and barren land covers tend to increase by an elevation increase. It can be concluded that high lands increased the variability of mean LST ratios. In cereal cropland cover, such a relationship was not very clear.

5. Modeling LST Mean Ratios by Multilinear Regression

The defined regression models in this study for each land cover classes recruited VZA, azimuth angle, slope, aspect, and elevation as independent variables and mean LST ratios in the training dataset were regarded as dependent variables (Table 2). Since VZA and slope has normal angle and azimuth and aspect has a horizontal angle, their difference was used to reduce the dependency among variables. Model evaluation was tested by using the Root Mean Square (RMSE) on the test dataset. Figure 13 showed the RMSEs in each observation time for different land covers. The RMSE of the model in barren land cover was the least for both satellite pairs in each observation time. Shrub, grass, and cereal crops had the low rankings, respectively. Also, the Figure 13 shows that the MODIS-Imager pair had lower RMSEs than MODIS-SEVIRI. For both sensor pairs, nightly observations had higher RMSEs in contrast with daily ones.

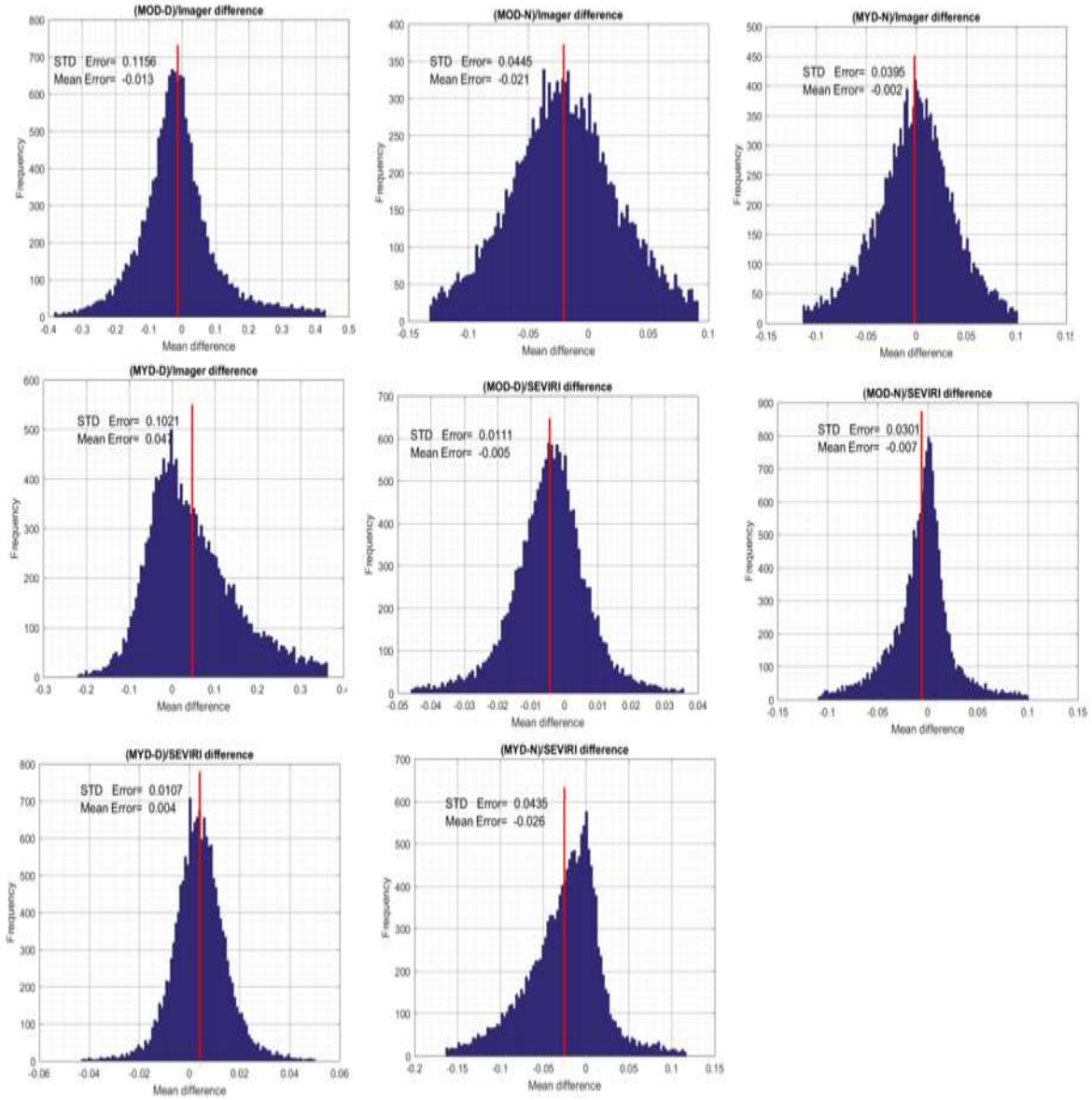

Figure 8. Error histogram of difference estimated MODIS-Imager and MODIS-SEVIRI mean ratios for two consequent periods

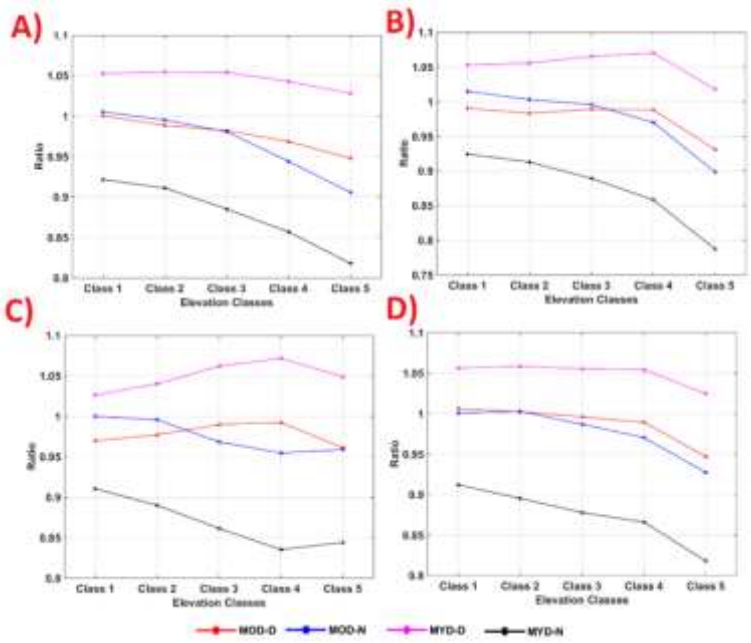

Figure 9. Mean LST ratio of MODIS-Imager for different land covers A) shrub, B) grass, C) cereal crop, D) barren or sparse vegetation

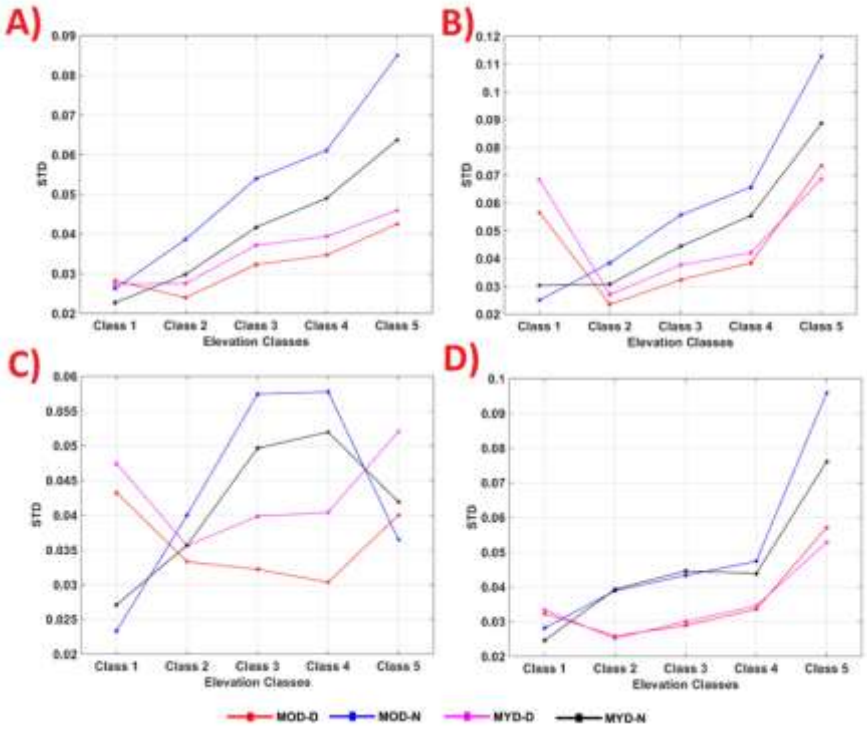

Figure 10. STD of mean LST ratios MODIS -imager for different land covers and elevations. A) shrub, B) grass, C) cereal crop, D) barren or sparse vegetation

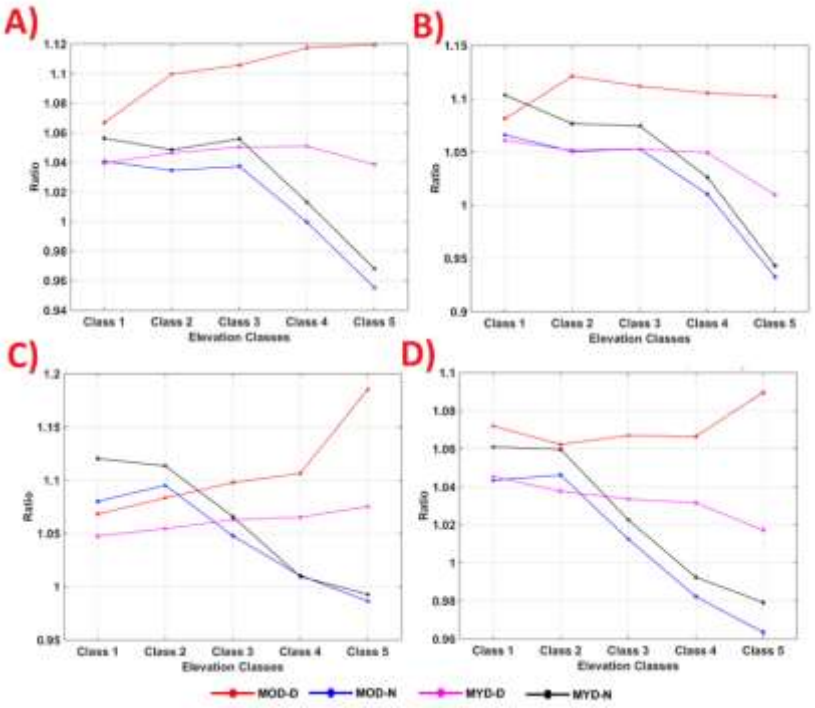

Figure 11. Mean LST ratio quantities of MODIS-SEVIRI for different land covers and elevation classes. A) shrub, B) grass, C) cereal crop, D) barren or sparse vegetation

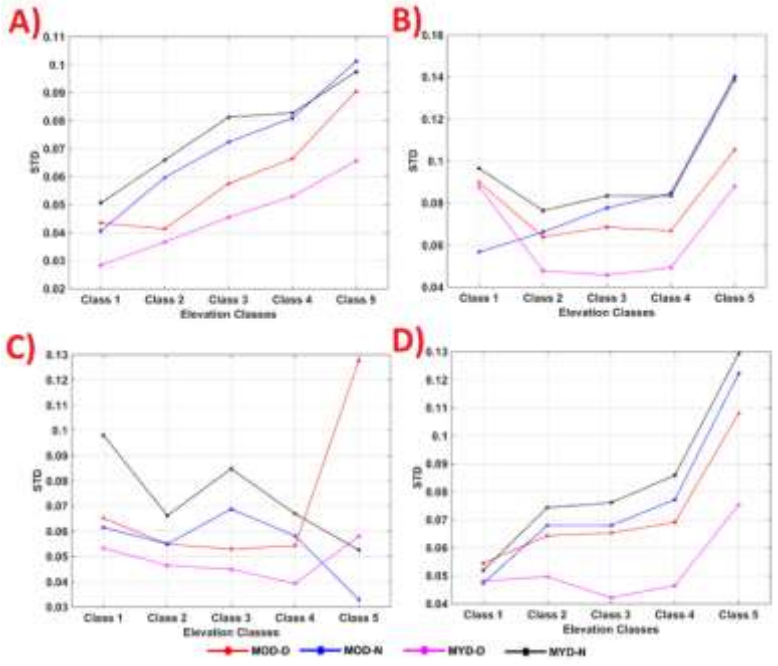

Figure 12. Standard deviation of mean LST ratios of MODIS -Imager for different land covers and elevations. A) shrub, B) grass, C) cereal crop, D) barren or sparse vegetation

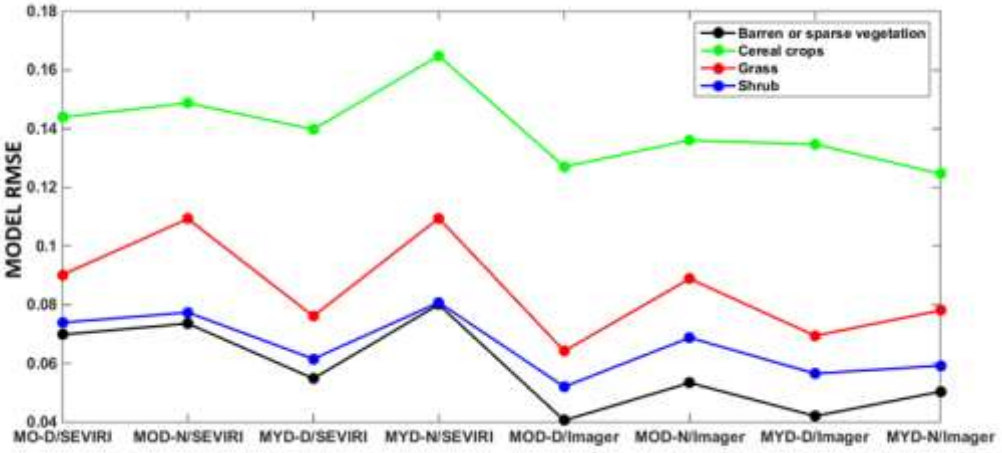

Figure 13. RMSEs for each observation time in different land covers

Table 2. Multi-linear regression coefficients for (VZA-slope), (azimuth-aspect), and elevation to model mean MODIS/SEVIRI and MODIS/Imager in different land covers.

Barren or sparse vegetation classes:		
MOD_N/SEVIRI	=	0.969 +0.0019(VZA-Slope) + 0.000482 (Azimuth-Aspect) +8.43e-07 (Elevation)
MYD_D/SEVIRI	=	1.1408 -0.0033(VZA-Slope) +7.45e-05 (Azimuth-Aspect) -3.77e-05 (Elevation)
MYD_N/SEVIRI	=	1.0487 -0.0013(VZA-Slope) +0.000281 (Azimuth-Aspect) -3.47e-06 (Elevation)
MOD_D/Imager	=	1.1676 -0.0035(VZA-Slope) -4.67e-06 (Azimuth-Aspect) -4.21e-05 (Elevation)
MOD_N/Imager	=	1.0884 -0.0016(VZA-Slope) +0.000177 (Azimuth-Aspect) -4.48e-06 (Elevation)
MYD_D/Imager	=	1.0317 -0.0002(VZA-Slope) +0.000228 (Azimuth-Aspect) -2.08e-05 (Elevation)
MYD_N/Imager	=	1.1021 -0.0009(VZA-Slope) +0.000184 (Azimuth-Aspect) +3.57e-06 (Elevation)
MOD_N/SEVIRI	=	0.8576 +0.0012(VZA-Slope) -0.000129 (Azimuth-Aspect) -3.12e-05 (Elevation)
Grass classes:		
MOD_N/SEVIRI	=	0.97619+0.0011(VZA-Slope) +0.0008(Azimuth-Aspect) +1.1e-05(Elevation)

MYD_D/SEVIRI	=	1.2051-0.0054(VZA-Slope) +0.00056(Azimuth-Aspect) -3.3e-05(Elevation)
MYD_N/SEVIRI	=	1.0971-0.003(VZA-Slope) +0.00043(Azimuth-Aspect) +7.7e-06(Elevation)
MOD_D/Imager	=	1.3009-0.0058(VZA-Slope) -8e-05(Azimuth-Aspect) -4.2e-05(Elevation)
MOD_N/Imager	=	1.1871-0.0038(VZA-Slope) -0.0001(Azimuth-Aspect) -9.4e-06(Elevation)
MYD_D/Imager	=	1.1912-0.0027(VZA-Slope) +0.00035(Azimuth-Aspect) -4.1e-05(Elevation)
MYD_N/Imager	=	1.1981-0.0029(VZA-Slope) -0.00018(Azimuth-Aspect) +2.6e-06(Elevation)
MOD_N/SEVIRI	=	1.0249-0.0012(VZA-Slope) -0.00034(Azimuth-Aspect) -6.5e-05(Elevation)

Shrub classes:

MOD_N/SEVIRI	=	0.98371+0.0011(VZA-Slope) +0.00062(Azimuth-Aspect) +2.1e-05(Elevation)
MYD_D/SEVIRI	=	1.1622+-0.0049(VZA-Slope) +0.00044(Azimuth-Aspect) -1.6e-05(Elevation)
MYD_N/SEVIRI	=	1.0485+-0.0017(VZA-Slope) +0.00048(Azimuth-Aspect) +1.1e-05(Elevation)
MOD_D/Imager	=	1.2231+-0.0056(VZA-Slope) +0.00013(Azimuth-Aspect) -1.4e-05(Elevation)
MOD_N/Imager	=	1.1257+-0.0025(VZA-Slope) +7.9e-05(Azimuth-Aspect) -7e-06(Elevation)
MYD_D/Imager	=	1.0951+-0.001(VZA-Slope) +0.0008(Azimuth-Aspect) -3.4e-05(Elevation)
MYD_N/Imager	=	1.1508+-0.0019(VZA-Slope) +0.00011(Azimuth-Aspect) +6.1e-07(Elevation)
MOD_N/SEVIRI	=	0.90484+0.0006(VZA-Slope) -0.00018(Azimuth-Aspect) -4.5e-05(Elevation)

Cereal crops classes:

MOD_N/SEVIRI	=	0.965+0.00187(VZA-Slope) +0.000233(Azimuth-Aspect) +3.78e-05(Elevation)
MYD_D/SEVIRI	=	1.285-0.00597(VZA-Slope) -0.000764(Azimuth-Aspect) -1.09e-06(Elevation)
MYD_N/SEVIRI	=	0.986+0.000518(VZA-Slope) +0.000331(Azimuth-Aspect) +2.23e-05(Elevation)
MOD_D/Imager	=	1.332-0.00681(VZA-Slope) -0.000849(Azimuth-Aspect) -5.78e-06(Elevation)
MOD_N/Imager	=	0.997-0.000742(VZA-Slope) -0.000126(Azimuth-Aspect) +1.67e-05(Elevation)
MYD_D/Imager	=	0.968+0.000666(VZA-Slope) -8.02e-05(Azimuth-Aspect) -2.27e-05(Elevation)
MYD_N/Imager	=	0.998+0.000217(VZA-Slope) -0.000209(Azimuth-Aspect) +3.06e-05(Elevation)
MOD_N/SEVIRI	=	0.838+0.00176(VZA-Slope) +8.4e-05(Azimuth-Aspect) -4.16e-05(Elevation)

6. Discussion

Overall, analysis of MODIS-Imager means LST ratio showed that MYD-D had larger LST values than Imager and MYD-N had lower LST values than Imager. Considering that the ratios can be temporally different, the ratios were tested between two datasets and showed that the ratio results can be the same in any period (Figure 8). Land surface emissivity from MODIS which are 10 major land cover classifications (EPSA 2014). The first variable in Imager LST retrieval is for the tropical regions. Therefore, the nature of such ratio in different land covers may be attributed to different lower atmospheric boundary temperatures in Iran. In MOD-D and MOD-N observation times, ratio values were close to one in flatlands. It can be concluded that in high and low temperatures, Imager had more errors. Also, general trends of mean LST ratios showed that by increasing elevation, the ratios reduce; Imager had larger LST values than MODIS in high elevation classes in all land covers. Such behavior may suggest the effects of topographic variables like aspect and slope. In standard deviation plots, the role of topography in LST variability in both sensors was shown.

The MODIS-SEVIRI mean LST ratios showed that time of day (temperature value) is an important factor in LST ratios when elevation increased; For lower temperatures (MOD-N and MYD-N) the ratios expressed the same trend of SEVIRI overestimation for higher elevation classes (fourth and fifth elevation classes). As the effects of elevation and land cover in each time had specific behaviors, for each land cover class a multi regression model was proposed based on azimuth, slope, aspect, VZA, and elevation. The regression validation through the test dataset showed low RMSEs in barren, shrub, grass, and cereal crops respectively. This can be concluded that vegetation is an important factor in LST discrepancies. Also, MODIS- Imager multi regression modeling had lower RMSEs in contrast with MODIS-SEVIRI.

7. Conclusion

Measurement of LST using geostationary satellite imagery can provide a suitable temporal resolution that can be applied in many applications such as meteorology, climatology, and hydrology modeling. MODIS-Imager means LST ratio analysis showed that during daytime Imager underestimates and during night time overestimates the LST. MODIS-SEVIRI mean LST ratios showed that in both day and night SEVIRI underestimates the LST for flatlands. Analysis of mean LST ratios in both pairs of sensors showed that land cover, time, and elevation were important factors. In fact, the effects of all these parameters were combined. The regression model evaluation showed that in barren land covers the MODIS-Imager and MODIS-SEVIRI had low discrepancies with model fitting. This can be concluded that desert areas can be suitable candidates for satellite calibration and study of different related environmental variables. The fitted model can be used as a calibration source for high temporal resolution LST data from both SEVIRI and Imager over Iran. Therefore, the accuracy of studies that use LST data can be improved.

Acknowledgments

The authors would like to appreciate NASA/USGS and Meteorological and Oceanographic Satellite Data Archival Centre (MOSDAC) for providing access to MOD11A1 product and INSAT3-D LST products. The authors deeply thank the Iranian National Science Foundation and the Iranian National Space Administration for their great supports in conducting this research.

References

Alavipanah, S., Komaki, C. B., Karimpour, R. M., Sarajian, M., Savaghebi, F. G. R., & Moghimi, E. (2007). Land surface temperature in the Yardang region of Lut Desert (Iran) based on field measurements and Landsat thermal data.

Aminou, D. (2002). MSG's SEVIRI instrument. *ESA Bulletin(0376-4265)*(111), 15-17.

EPSA. Insat-3d Algorithm Theoretical Basis Document. Space Applications Centre, Government of India (2014).

Gao, C., Jiang, X., Wu, H., Tang, B., Li, Z., & Li, Z. (2012). Comparison of land surface temperatures from MSG-2/SEVIRI and Terra/MODIS. *Journal of Applied Remote Sensing, 6*(1), 063606.

Golestanil, Y., Noorian, A.-M., & Hudak, D. (2000). Design considerations for the two C-and one S-band doppler weather radars in the Islamic Republic of Iran. *Physics and Chemistry of the Earth, Part B: Hydrology, Oceans and Atmosphere, 25*(10-12), 991-994.

Jin, M. (2004). Analysis of land skin temperature using AVHRR observations. *Bulletin of the American Meteorological Society, 85*(4), 587-600.

Katiraie-Boroujerdy, P.-S., Nasrollahi, N., Hsu, K.-l., & Sorooshian, S. (2013). Evaluation of satellite-based precipitation estimation over Iran. *Journal of arid environments, 97*, 205-219.

Li, Z.-L., Tang, B.-H., Wu, H., Ren, H., Yan, G., Wan, Z., . . . Sobrino, J. A. (2013). Satellite-derived land surface temperature: Current status and perspectives. *Remote sensing of environment, 131*, 14-37.

Norman, J. M., & Becker, F. (1995). Terminology in thermal infrared remote sensing of natural surfaces. *Agricultural and Forest Meteorology, 77*(3-4), 153-166.

Pandya, M., Shah, D., Trivedi, H., & Panigrahy, S. (2011). Simulation of at-sensor radiance over land for proposed thermal channels of Imager payload onboard INSAT-3D satellite using MODTRAN model. *Journal of earth system science, 120*(1), 19-25.

RMI Team, LSA SAF. The Eumetsat Satellite Application Facility on Land Surface Analysis (Lsa Saf). Damstadt, 2011.

Sobrino, J., & Romaguera, M. (2004). Land surface temperature retrieval from MSG1-SEVIRI data. *Remote sensing of environment, 92*(2), 247-254.

Tang, H., & Li, Z.-L. (2013). *Quantitative remote sensing in thermal infrared: theory and applications*: Springer Science & Business Media.

Trigo, I. F., Monteiro, I. T., Olesen, F., & Kabsch, E. (2008). An assessment of remotely sensed land surface temperature. *Journal of Geophysical Research: Atmospheres, 113*(D17).

Wan, Zhengming. (2016). *Collection-6, Modis Land Surface Temperature Products. Users' Guide*. University of California, Santa Barbara.

Wan, Zhengming. (2006). *Modis Land Surface Temperature Products Users' Guide*. Institute for Computational Earth System Science, University of California, Santa Barbara, CA.

Wan, Zhengming. (2008). New refinements and validation of the MODIS land-surface temperature/emissivity products. *Remote sensing of environment, 112*(1), 59-74.

Wan, Z., & Dozier, J. (1996). A generalized split-window algorithm for retrieving land-surface temperature from space. *IEEE Transactions on geoscience and remote sensing, 34*(4), 892-905.

Wang, A., Barlage, M., Zeng, X., & Draper, C. S. (2014). Comparison of land skin temperature from a land model, remote sensing, and in situ measurement. *Journal of Geophysical Research: Atmospheres, 119*(6), 3093-3106.

Weng, Q. (2009). Thermal infrared remote sensing for urban climate and environmental studies: Methods, applications, and trends. *ISPRS Journal of Photogrammetry and Remote Sensing, 64*(4), 335-344.

Xu, T., Liu, S., Liang, S., & Qin, J. (2011). Improving predictions of water and heat fluxes by assimilating MODIS land surface temperature products into the common land model. *Journal of Hydrometeorology, 12*(2), 227-244.